Regional Extreme Precipitation Events in Wintertime Japan Facilitated by East-Asian Large-Scale Flow Patterns

Takumi Matsunobu[1, 2], Julian F. Quinting[3], Christian M. Grams[3], and Mio Matsueda[4]

[1]*Meteorologisches Institut*, *Ludwig-Maximilians-Universität München*, *Munich*, *Germany*
[2]*Graduate School of Science and Technology*, *University of Tsukuba*, *Tsukuba*, *Japan*
[3]*Institute of Meteorology and Climate Research (IMK-TRO)*, *Karlsruhe Institute of Technology*, *Karlsruhe*, *Germany*
[4]*Center for Computational Sciences*, *University of Tsukuba*, *Tsukuba*, *Japan*

(Manuscript received 2 June 2023, accepted 1 September 2023)

Abstract The statistical and dynamical relationships between regional extreme precipitation events (EPEs) during wintertime in five Japanese regions and East-Asian synoptic weather patterns are addressed. Two of the five weather patterns, the southerly flow (SF) and low pressure (LP), are associated with about 50% of EPEs in all the regions. A regional dependency is found, with SF being more likely to cause extreme precipitation in two regions in the south of Japan and LP in the other regions, respectively. The large-scale dynamics leading to EPEs in each region are assessed by a combined Lagrangian and Eulerian analysis. In the two southern regions, EPEs are predominantly associated with direct moisture supply from the subtropical oceans. This is modulated by the large-scale flow pattern of SF. In contrast, EPEs in the northern coastal areas of the Sea of Japan and the Pacific Ocean are influenced by anomalous moisture supply from the cyclone-induced moisture convergence modulated by LP. The eastern coastal region of the Sea of Japan shows a mixture of both these moisture supply mechanisms. The strong link between EPEs and synoptic patterns might help to improve predictions of extreme events, even on the sub-seasonal forecast skill horizon.

Citation: Matsunobu, T., J. F. Quinting, C. M. Grams, and M. Matsueda, 2023: Regional extreme precipitation events in wintertime Japan facilitated by East-Asian large-scale flow patterns. *SOLA*, **19**, 253−260, doi:10.2151/sola.2023-033.

1. Introduction

Severe weather events have detrimental impacts on economic and social infrastructure. Increasing trends of intense precipitation in Japan under a warming climate have been reported (Groisman et al. 2005; Fujibe et al. 2006; Donat et al. 2016; So et al. 2022). Duan et al. (2014) demonstrated that relatively weak, successive precipitation events show a decreasing trend, and 1- and 5-day precipitation has become more intense in the last couple of decades.

Large-scale circulation is—in principle—more predictable than local extreme precipitation events (EPEs) at longer forecast lead times (Buizza and Leutbecher 2015; Khain et al. 2020). At different temporal and spatial scales the modulation of local weather by large-scale flow patterns has been investigated (Beerli and Grams 2019; Pasquier et al. 2019; Domeisen et al. 2020; Miyasaka et al. 2020; Mastrantonas et al. 2021; Sawada and Ueno 2021). For instance, Pfahl and Wernli (2012) suggests that 80% of EPEs over Japan during winter are enforced by cyclonic flow systems.

To detect flow patterns, a widely used method is stratifying the large-scale flow using statistical clustering, resulting in so-called "weather regimes" or "weather patterns" that recur frequently and persist for a long time, providing longer predictability (Yiou and Nogaj 2004; 39 Ferranti et al. 2015; Matsueda and Kyouda 2016; White et al. 2022). This approach is attractive to national weather services as well as the energy sector due to its potential for extending the forecast skill horizon (Grams et al. 2017; Lavaysse et al. 2018; White et al. 2022). Understanding the link between wintertime EPEs in Japan and large-scale flow patterns in the upper atmosphere can help predict EPEs far in advance and mitigate socio-economic impacts.

This study aims to explore the statistical and dynamical link between wintertime EPEs in various regions of Japan and East-Asian synoptic weather patterns. Section 2 describes the data and methods. Sections 3.1 and 3.2 explore the statistical relationship between EPEs and weather patterns. In Sections 3.3 and 3.4, we explore the synoptic situation during EPEs and the effect of anomalous large-scale flows facilitating EPEs. Section 4 summarises our findings.

2. Data and method

We use the European Centre for Medium-range Weather Forecasts (ECMWF) Re-Analysis 5 dataset (ERA5; Hersbach et al. 2020) for synoptic analyses and the ground-based observations called AMeDAS (the Automated Meteorological Data Acquisition System) (JMA 2023) for 20-km interval precipitation data over Japan (Section 2.2). ERA5

Corresponding author: Mio Matsueda, Center for Computational Sciences, University of Tsukuba, 305-8577 Tsukuba, Japan. E-mail: mio@ccs.tsukuba.ac.jp.

fields are remapped to 1.25° latitude–longitude grid, except for the Lagrangian analysis (Section 2.3). Forty extended winters (November–March during 1979/80 to 2018/19, 365-day calendar) are investigated.

2.1 Definition of East-Asian synoptic weather patterns

We define East-Asian synoptic weather patterns based on Matsueda and Kyouda (2016, hereafter MK2016). Using *k*-means clustering for pattern detection (Jung et al. 2005), samples are divided into five categories based on the inherent characteristics of the samples. Clustering is applied to top 20 non-normalised principal components of the 500-hPa geopotential height field (Z500) over the East-Asian region (20°N–60°N, 100°E–170°E) at 12 UTC. Each day within the span of 40 winters (a total of 6040 days) is attributed to one of the five patterns.

2.2 Identification of extreme precipitation events

In this study, an EPE is a day with daily accumulated precipitation averaged over AMeDAS observations in a region exceeding a threshold. We defined the five regions in Japan according to the seasonal forecast regions of the Japan Meteorological Agency (JMA 2022): Southwestern Japan (SWJ), the Pacific coasts of Eastern Japan (PEJ) and Northern Japan (PNJ), and the Japan Sea coasts of Eastern Japan (JEJ) and Northern Japan (JNJ) (Fig. 2). A change from the reference is merging the two western Japan regions into SWJ.

For EPE days, the 90th percentile of daily precipitation sets the threshold. Daily accumulation is the sum of 00–24 UTC precipitation at each AMeDAS station, omitting days with 6 hours or more of missing data. This yields data from 1317 AMeDAS stations across 40 winters (station counts: 442 in SWJ, 283 in PEJ, 276 in PNJ, 109 in JEJ, 207 in JNJ). Area-average daily precipitation is calculated as the mean of the stations per region. Using the 90th percentile threshold, 604 EPEs are selected for each region.

2.3 Trajectory calculations

To investigate the origin of air masses associated with extreme rainfall, 3-day backward trajectories are computed using a Lagrangian analysis tool (Lagranto; Sprenger and Wernli 2015). The computations are based on ERA5's three-dimensional wind fields at all available model levels that were derived on a regular 0.5° × 0.5° latitude–longitude grid every 3 hours. The trajectories are started at 12 UTC on each day of an EPE from grid points lying at an equidistant grid of 60 km × 60 km inside the five regions and from 17 equidistant pressure levels ranging from 970 to 490 hPa. Following Sodemann et al. (2008), we assume that the relative humidity of precipitating air parcels exceeds 80% at their starting time. Accordingly, we consider only those trajectories starting at grid points where this criterion is fulfilled. In the last step, the trajectories are gridded at each time step on a regular 1° × 1° latitude–longitude grid in order to display their density at various time steps prior to the EPE.

3. Results

3.1 Synoptic weather patterns

We identify five East-Asian weather patterns that reflect those of MK2016 (Fig. 1): winter monsoon (WM), western Pacific (WP), high pressure (HP), low pressure (LP), and southerly flow (SF). This supports the robustness of the clustering and its insensitivity to differences in re-analysis datasets, although slight differences are found: the centre of the negative anomaly during WM has shifted slightly eastward and the occurrence frequency of LP increased by 1.8%, decreasing the other frequencies by 0.2–0.7%. The more frequent appearance of LP in the late 2010s leads to a change in the entire period (not shown). Further description of the weather patterns is found in Supplementary Text S1.

3.2 EPEs' Relationship to the East-Asian weather patterns

To elucidate the extent to which East-Asian weather patterns are linked to EPEs, we calculate the frequencies of the five weather patterns during the occurrence of EPEs in each region (Fig. 3a and Supplementary Table S1 for detailed numbers). In all regions, more than 50% of EPEs happen on a day of SF or LP. SF constitutes 50% and 44% of all extreme days in SWJ and PEJ, respectively, and LP is the second most frequent pattern during EPEs in these regions. In contrast, LP plays an important role in the northern regions; i.e., JEJ, JNJ, and PNJ. LP is the prevailing weather pattern for 32%, 38%, and 38% of all EPE cases in JEJ, JNJ, and PNJ, respectively. During the other three patterns (WM, WP, and HP), EPEs occur less frequently. In JEJ and JNJ, WM and WP constitute relatively higher fractions, but their occurrence frequencies are comparable with the climatological ones. Precipitation patterns for EPEs in these regions show a curvature of the typical monsoonal effect, as shown in the third and fourth rows of Supplementary Fig. S1. However, LP still has more EPE cases there. This result gives us additional insight into Pfahl and Wernli (2012). The northern regions seem to coincide with their conclusion, but in the southern regions a different flow characteristic seems to be at play.

A question that naturally follows is, whether a certain weather pattern enhances the likelihood of an EPE. A differ-

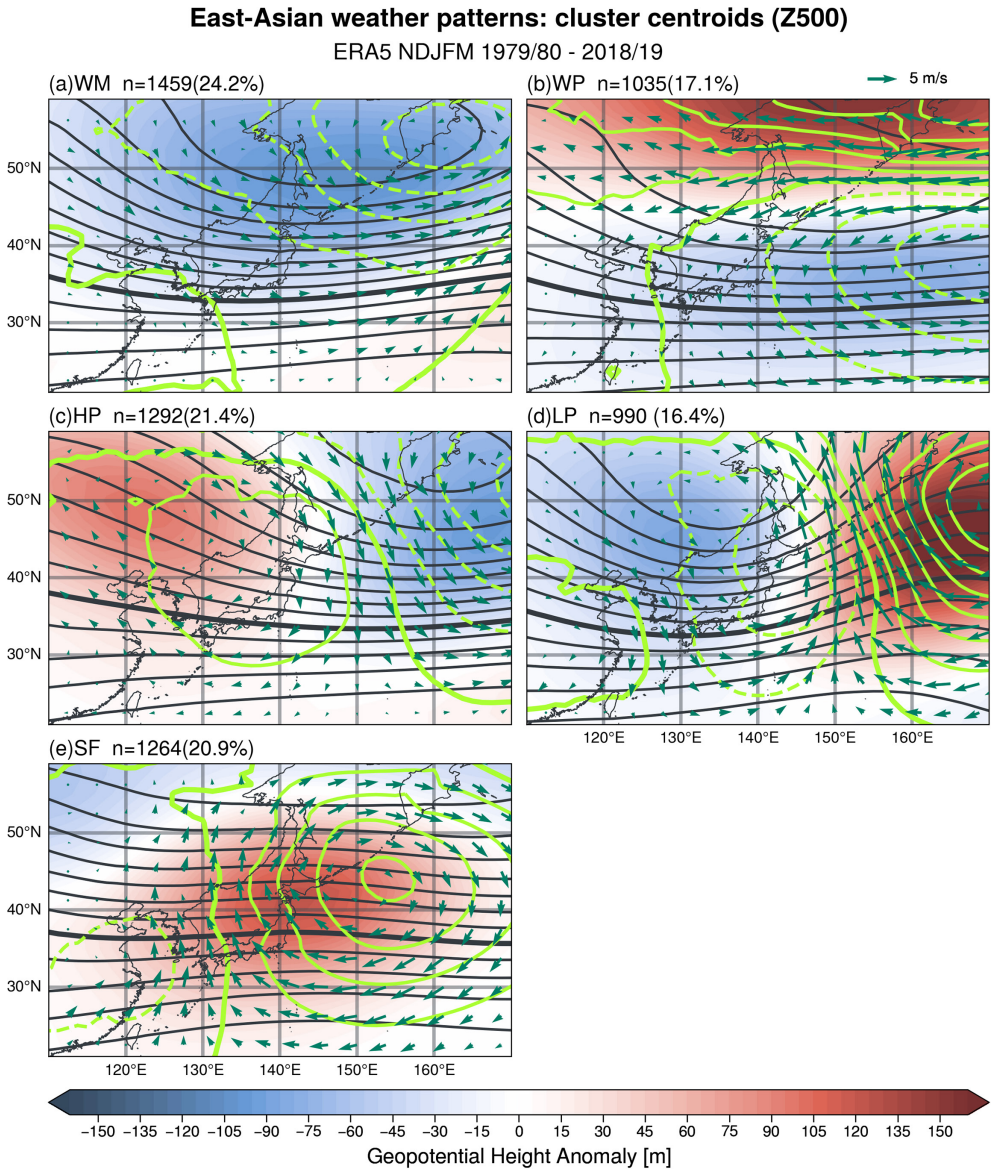

Fig. 1. Geopotential height anomaly of each cluster centroid (shading) and mean geopotential height of each weather pattern (black contours; every 60 m with thick contour denoting 5600-m isoline) at 500-hPa pressure level. Mean anomalous sea level pressure is drawn by light green contours. Arrows indicate mean anomalous winds at a pressure level of 850 hPa (reference vector is given in the top right corner). The number of days on which each pattern *n* was detected and the climatological occurrence frequency are indicated in each panel heading.

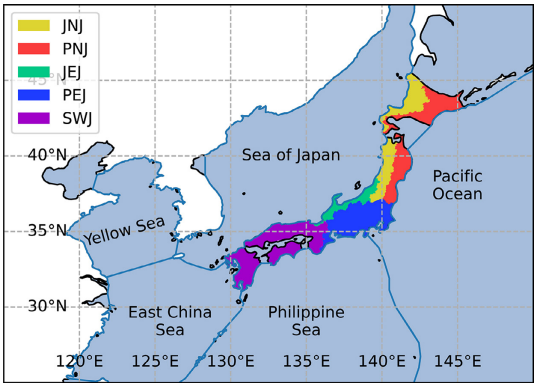

Fig. 2. Map of five regions of Japan (coloured) and Oceans (blue lines) used for the backward trajectory analysis.

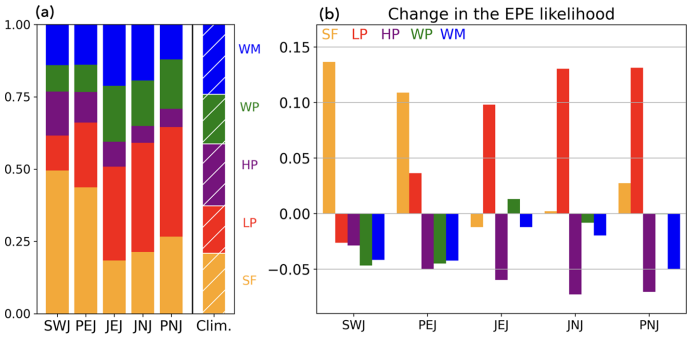

Fig. 3. (a) Occurrence frequency of weather patterns during EPEs in each region. The hatched bar on the right indicates the climatological frequencies. (b) Change in the likelihood of EPE occurrence in each region from the climatological occurrence frequency (~0.10).

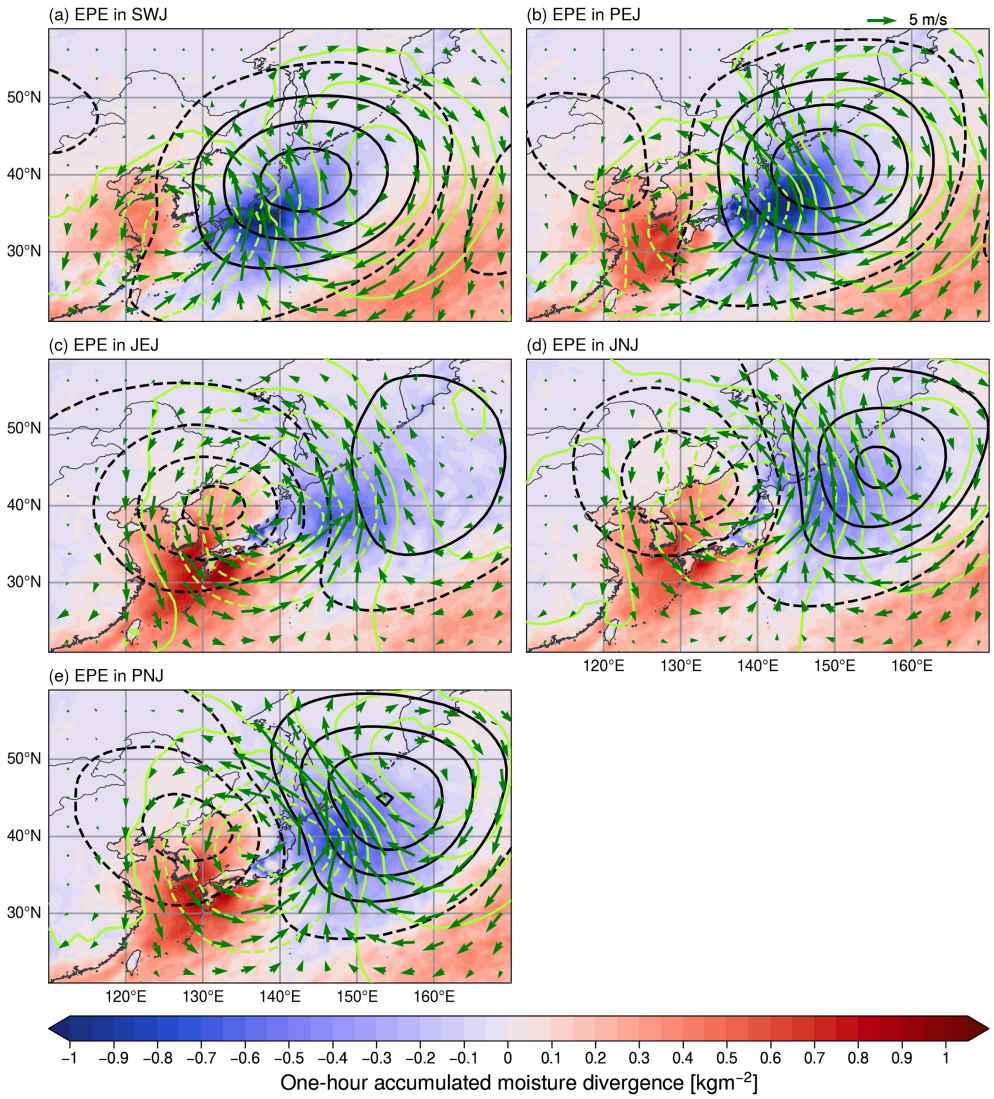

Fig. 4. Mean one-hour accumulated moisture divergence (shading in kg m^{-2}) vertically integrated over the entire atmosphere. A red and blue colour indicates an increase and decrease in moisture, respectively. Arrows indicate mean anomalous winds at a pressure level of 850 hPa (reference vectors are given in the upper right corner). Black contours indicate mean geopotential height anomaly at a pressure level of 500 hPa (every 60 m), light green mean anomalous sea level pressure (every 2 hPa). All fields are averaged over 12 UTC of extreme precipitation days in each region.

ence in EPE occurrence frequency from the climatology indicates an increased or reduced likelihood of EPE occurrence given the weather pattern. The change in the likelihood of EPE occurrence in each region is illustrated in Fig. 3b (Supplementary Table S2 for values). Apparently, SF has a profound impact in SWJ and PEJ, whilst LP dominates in the other part of Japan. Those impacts almost double the likelihood. PNJ, JEJ and JNJ are more sensitive to LP, which enhances EPEs, and HP, which suppresses them, representing migrating wave patterns with the waveguide over the northern regions (Figs. 1c and 1d). Despite the stronger monsoon effect expected with WM and WP in JEJ and JNJ, these patterns show a very slight increase in the EPE likelihood only in JEJ. A clear message obtained here is that EPEs favour the synoptic patterns of SF and LP and vice versa, and this is strongly region dependent.

3.3 Background dynamics

The investigation in Section 3.2 showed that SF increases the occurrence of EPE in SWJ and PEJ, and LP in PNJ, JEJ and JNJ. To understand how EPEs are dynamically linked with the large-scale flows of SF and LP, we investigate the synoptic composites of EPE days in this section.

A comparison of the composites of anomalous sea level pressure (SLP) and wind in Fig. 4 with those in Fig. 1 demonstrates the influence of the weather patterns for EPEs. The dipole pattern of the west-to-east SLP anomaly and the southerly flow anomaly appear to be the common synoptic features for all regions. On closer inspection, however, we can see that their relationship to the weather patterns varies. The black contours during EPE in SWJ and PEJ (Figs.

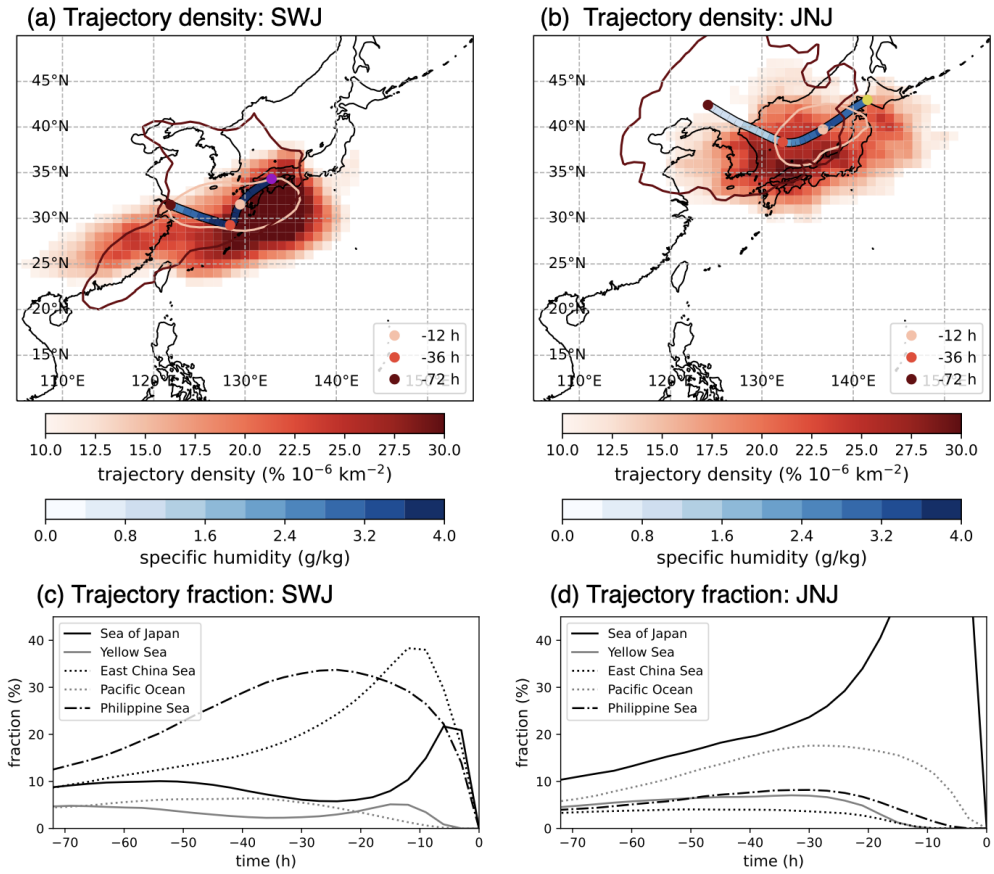

Fig. 5. Results of backward trajectory analysis for extreme precipitation events in the (a, c) SWJ and (b, d) JNJ regions. (a, b) Trajectory density is shown at −72 h by the dark red contour (contour at 10% 10^{-6} km^{-2}), at −36 h by red shading, and at −12 h by the light red contour (contour at 60% 10^{-6} km^{-2}). Mean trajectory is given as a thick blue line coloured by the average specific humidity (g kg^{-1}). (c, d) Fraction of trajectories over ocean basins surrounding Japan (see Fig. 2) as a function of time. The sum over the fractions does not yield 100%, as trajectories over land are not considered.

4a and 4b) show high geopotential anomaly over Japan, similar to those of SF (Fig. 1e). Likewise, EPEs in JEJ, JNJ and PNJ (Figs. 4c–4e) are characterised by an anomalous surface low pressure centred over mainland Japan, reminiscent of LP (Fig. 1d). The strong high SLP anomaly lies to the east of the high geopotential anomaly and involves a stronger southerly wind anomaly on the western flank. These are dominated by the elongated upper tropospheric anomaly originating from high latitudes, indicating the indirect influence of large-scale meridional interactions related to Rossby wave breaking (de Vries 2021).

As for the moisture transport, an anomalous convergent flow during EPEs in SWJ and PEJ appears to moisten directly over the affected region (dark blue in Figs. 4a and 4b). This is the result of a confluence of two moist anomalous air streams, mainly from the subtropical oceans, enforced by the wind anomaly associated with SF. The resulting confluence leads to an accumulation of moisture over the south of Japan that is then pushed towards the Japanese mainland. In contrast, for PNJ, JNJ and JEJ moisture convergence occurs east of the EPE regions over the Pacific Ocean (Figs. 4c–4e). This suggests that this cyclone-induced moisture convergence over the Pacific Ocean could contribute to EPEs in PNJ, JNJ and JEJ, which we will explore in more detail with the Lagrangian perspective in Section 3.4. Note that the strong convergence over the coastal area of the Sea of Japan is commonly found among the composites. This moisture supply is well known as the monsoon effect of wintertime Japan. However, this alone does not always cause precipitation extreme relative to the climatology (Yamashita et al. 2012). This is also implied by the neutral contribution of WM to the EPE likelihood shown in Fig. 3b.

3.4 Backward trajectory analysis

The Eulerian perspective on the synoptic flow configuration and moisture convergence during EPEs suggests that SF and LP enhance EPEs through different processes. To detect the possible source of moisture supply linked to the weather patterns, a backward trajectory analysis is performed for EPEs in all the regions (Section 2.3 for technical details). Figure 5 shows a result exemplarily for SWJ and JNJ, as a representative for SF- and LP-induced events, respectively. For completeness the analysis for PEJ, JEJ and JNJ are shown in Supplementary Figure S2.

Three days prior to EPEs in SWJ, air parcels are located in East Asia, over the East China Sea, the Philippine Sea, the Yellow Sea and the Sea of Japan (dark red contour in Figs. 5a and 5c). From there, they move to the south of 35°N 36 hours before the event (red shading). Clearly, the dense trajectory overlaps well with the moisture convergence shown in Fig. 4a, and the parcels' specific humidity is getting almost saturated by −36 h (blue line). This illustrates the path of the SF contribution to EPEs. These parcels are initially embedded over oceans surrounding the southern part of Japan. The marked increase in specific humidity identifies these subtropical oceans as local moisture sources once they reach the SWJ region with the help of anomalous flow from SF. Similarly, although the relative contributions of the oceans vary, southern oceans moisten the air parcels by 36 hours before EPEs in PEJ and the parcels are carried towards the region (Figs. S2a and S2d).

In contrast, the majority of air parcels involved in EPEs in JNJ originate mainly from northern China and Korea (dark red contour in Fig. 5b). The parcels follow a southeastward path until they spread over Japan and the surrounding oceans 36 hours prior to the events (red shading in Figs. 5b and 5d). The moisture increase along the trajectories is initially not pronounced, but it increases between 48 and 12 hours before the event (blue line in Fig. 5b), at which time the Pacific Ocean has a non-negligible fraction (Fig. 5d), where large-scale flows reinforce the moistening (Fig. 4e). This demonstrates that, unlike the confluence of moistened air parcels due to SF for SWJ and PEJ (Figs. 4a and 4b), the cyclone-induced moisture convergence over the Pacific Ocean along with the monsoon effect over the Sea of Japan contributes to EPEs in JNJ, consistent with previous studies (e.g. Yamashita et al. 2012; Ando and Ueno 2015). PNJ also seems to be affected by the cyclone-induced flow like JNJ (Figs. S2c and S2f). For JEJ (Figs. S2b and S2e) the trajectory analysis suggests more widespread air mass origin and moisture sources compared to the other regions. This is reminiscent of the partly cyclonic flow around the anomalous low in LP that ultimately reaches the region from the west (Fig. 4c). The JEJ region appears to have a mixed characteristic of direct moistening by the Sea of Japan and the cyclonic effect concerning moisture supplies.

4. Conclusions

In this study, we have assessed the statistical relationship between regional EPEs in wintertime Japan and the East-Asian weather patterns. The large-scale dynamics facilitating EPEs in five regions are also explored using composite and backward trajectory analysis.

More than 50% of EPEs are accompanied by either LP or SF. The individual contribution rate of these two patterns depends on the regions: in the SWJ and PEJ regions, SF comprises 44–50% of all cases, while in the other regions, JEJ, JNJ and PNJ, LP is the dominant weather pattern. The likelihood of EPE occurrence doubles during SF in SWJ and PEJ, whereas it more than doubles during LP for the other regions (Fig. 3b). Despite the known importance of the monsoon effect over the coastal area of the Sea of Japan, WM has little impact to enhance EPE only in JEJ.

The composite and backward trajectory analysis shed light on the different pathways causing EPEs in each region. In SWJ and PEJ, the synoptic SF-like flow brings moist warm air directly from subtropical oceans to the regions where EPEs occur. In JNJ and PNJ, on the other hand, cyclone-driven flows represented by LP converge eastward off Japan. Air parcels crossing there take up convergent moisture and transport anomalous moisture along with the monsoonal moisture supply over the Sea of Japan, which results in extreme precipitation. Our results corroborate the previous research on the effect of cyclonic flow (Pfahl and Wernli 2012) and upper-tropospheric Rossby wave (de Vries 2021), and add the regional dependence of these effects.

A caveat of our study is that it does not address the intra-regional variability of extreme precipitation, which is perceived in Supplementary Fig. S1. This is due to our focus on a statistical exploration of the large-scale impact rather than individual extremes at scales of O(10km). Other studies cover that point with a focus on local snowfall with point observations (e.g. with a convection-permitting model (Kawase et al. 2018) and observations at city scales in one region (Yamazaki et al. 2019)). Nevertheless, further investigation in the context of a coarse-grained approach as this work would expand our understanding.

We conclude that EPEs in wintertime Japan are to a large degree driven by the synoptic flows described by the simple patterns in the troposphere. The conclusion is consequently similar to those in other parts of the world (e.g. in the Mediterranean shown by Mastrantonas et al. 2021); nevertheless, the precise quantification enables us to benefit, for example, in the calibration of models' climatology and in obtaining a better picture of the effect of global warming. Another recent prospect is a dependence of local forecast skill on synoptic conditions (Keil et al. 2020; Büeler et al. 2021; Matsunobu et al. 2022; Nabizadeh et al. 2022). A follow-up study that will investigate this point should give further insight.

Acknowledgments

This work is a contribution to the "Weather regimes in Europe and Asia: Subseasonal Predictability" (WEASP) project funded by the Deutscher Akademischer Austauschdienst (DAAD) and the University of Tsukuba. TM acknowledges

support from the "Waves to Weather" (SFB/TRR 165) funded by the German Research Foundation (DFG). The work of JQ and CMG was funded by the Helmholtz Association as part of the Young Investigator Group, "Sub-seasonal Predictability: Understanding the Role of Diabatic Outflow" (SPREADOUT, grant VH-NG-1243). We thank Dominik Büeler and Akio Yamagami for inspiring discussions, and to Dr Yuhei Takaya and anonymous reviewers for valuable comments and suggestions, which helped to improve the quality of the manuscript. We thank the ECMWF and Deutscher Wetterdienst for granting access to the ERA5 datasets that are available from the Climate Data Store (CDS) at https://doi.org/10.24381/cds.bd0915c6. The Lagranto code is available at http://iacweb.ethz.ch/staff/sprenger/lagranto/.

Edited by: Y. Takaya

Supplements

Supplement 1: Supplementary File contains the list of dates with East-Asian weather patterns and EPE flags in each of the regions.

Supplement 2: In the PDF file, Supplementary Text S1 contains further descriptions of East-Asian weather patterns. Supplementary Text S2 describes the data format of Supplementary File. Supplementary Figure S1, S2, Supplementary Table S1 and S2 are also included.

References

Ando, N., and K. Ueno, 2015: Occurrence tendency of heavy rainfall or snowfall in the inland district of Japan in winter. *Seppyo*, **77**, 397–410 (in Japanese with an English abstract).

Beerli, R., and C. M. Grams, 2019: Stratospheric modulation of the large-scale circulation in the Atlantic–European region and its implications for surface weather events. *Quart. J. Roy. Meteor. Soc.*, **145**, 3732–3750.

Buizza, R., and M. Leutbecher, 2015: The forecast skill horizon. *Quart. J. Roy. Meteor. Soc.*, **141**, 3366–3382.

Büeler, D., L. Ferranti, L. Magnusson, J. F. Quinting, and C. M. Grams, 2021: Year-round sub-seasonal forecast skill for atlantic-european weather regimes. *Quart. J. Roy. Meteor. Soc.*, **147**, 4283–4309.

Domeisen, D. I. V., C. M. Grams, and L. Papritz, 2020: The role of north atlantic–european weather regimes in the surface impact of sudden stratospheric warming events. *Wea. Climate Dyn.*, **1**, 373–388.

Donat, M. G., A. L. Lowry, L. V. Alexander, P. A. O'Gorman, and N. Maher, 2016: More extreme precipitation in the world's dry and wet regions. *Nat. Climate Change 2016*, **6**, 508–513.

Duan, W., B. He, K. Takara, P. Luo, M. Hu, N. E. Alias, and D. Nover, 2014: Changes of precipitation amounts and extremes over japan between 1901 and 2012 and their connection to climate indices. *Climate Dyn.*, **45**, 1–20.

Ferranti, L., S. Corti, and M. Janousek, 2015: Flow-dependent verification of the ecmwf ensemble over the euro-atlantic sector. *Quart. J. Roy. Meteor. Soc.*, **141**, 916–924.

Fujibe, F., N. Yamazaki, and K. Kobayashi, 2006: Long-term changes of heavy precipitation and dry weather in Japan (1901–2004). *J. Meteor. Soc. Japan*, **84**, 1033–1046.

Grams, C. M., R. Beerli, S. Pfenninger, I. Staffell, and H. Wernli, 2017: Balancing Europe's wind-power output through spatial deployment informed by weather regimes. *Nat. Climate Change*, **7**, 557–562.

Groisman, P. Y., R. W. Knight, D. R. Easterling, T. R. Karl, G. C. Hegerl, and V. N. Razuvaev, 2005: Trends in intense precipitation in the climate record. *J. Climate*, **18**, 1326–1350.

Hersbach, H., B. Bell, P. Berrisford, S. Hirahara, A. Horányi, J. Muñoz-Sabater, J. Nicolas, C. Peubey, R. Radu, D. Schepers, A. Simmons, C. Soci, S. Abdalla, X. Abellan, G. Balsamo, P. Bechtold, G. Biavati, J. Bidlot, M. Bonavita, G. De Chiara, P. Dahlgren, D. Dee, M. Diamantakis, R. Dragani, J. Flemming, R. Forbes, M. Fuentes, A. Geer, L. Haimberger, S. Healy, R. J. Hogan, E. Hólm, M. Janisková, S. Keeley, P. Laloyaux, P. Lopez, C. Lupu, G. Radnoti, P. de Rosnay, I. Rozum, F. Vamborg, S. Villaume, and J. N. Thépaut, 2020: The ERA5 global reanalysis. *Quart. J. Roy. Meteor. Soc.*, **146**, 1999–2049.

JMA, 2022: *Forecast divisions used in seasonal forecasting* (Available online at: https://www.jma.go.jp/jma/en/Activities/amedas/amedas.html, accessed 12 September 2022).

JMA, 2023: *AMeDAS* (Available online at: https://www.jma.go.jp/jma/en/Activities/amedas/amedas.html, accessed 31 March 2023).

Jung, T., T. N. Palmer, and G. J. Shutts, 2005: Influence of a stochastic parameterization on the frequency of occurrence of North Pacific weather regimes in the ECMWF model. *Geophys. Res. Lett.*, **32**, L23811.

Kawase, H., T. Sasai, T. Yamazaki, R. Ito, K. Dairaku, S. Sugimoto, H. Sasaki, A. Murata, and M. Nosaka, 2018: Characteristics of synoptic conditions for heavy snowfall in western to northeastern japan analyzed by the 5-km regional climate ensemble experiments. *J. Meteor. Soc. Japan. Ser. II*, **96**, 161–178.

Keil, C., L. Chabert, O. Nuissier, and L. Raynaud, 2020: Dependence of predictability of precipitation in the northwestern mediterranean coastal region on the strength of synoptic control. *Atmos. Chem. Phys.*, **20**, 15851–15865.

Khain, P., Y. Levi, A. Shtivelman, E. Vadislavsky, E. Brainin, and N. Stav, 2020: Improving the precipitation forecast over the eastern mediterranean using a smoothed time-lagged ensemble. *Meteor. Appl.*, **27**, e1840.

Lavaysse, C., J. Vogt, A. Toreti, M. L. Carrera, and F. Pappenberger, 2018: On the use of weather regimes to forecast meteorological drought over europe. *Nat. Hazards Earth Syst. Sci.*, **18**, 3297–3309.

Mastrantonas, N., P. Herrera-Lormendez, L. Magnusson, F. Pappenberger, and J. Matschullat, 2021: Extreme precipitation events in the mediterranean: Spatiotemporal characteristics and connection to large-scale atmospheric flow patterns. *Int. J. Climatol.*, **41**, 2710–2728.

Matsueda, M., and M. Kyouda, 2016: Wintertime East Asian flow patterns and their predictability on medium-range timescales. *SOLA*, **12**, 121–126.

Matsunobu, T., C. Keil, and C. Barthlott, 2022: The impact of microphysical uncertainty conditional on initial and boundary condition uncertainty under varying synoptic control. *Wea. Climate Dyn.*, **3**, 1273–1289.

Miyasaka, T., H. Kawase, T. Nakaegawa, Y. Imada, and I. Takayabu, 2020: Future projections of heavy precipitation in kanto and associated weather patterns using large ensemble high-resolution simulations. *SOLA*, **16**, 125–131.

Nabizadeh, E., S. W. Lubis, and P. Hassanzadeh, 2022: The summertime pacific-north american weather regimes and their predictability. *Geophys. Res. Lett.*, **49**, e2022GL099401.

Pasquier, J. T., S. Pfahl, and C. M. Grams, 2019: Modulation of atmospheric river occurrence and associated precipitation extremes in the north atlantic region by european weather regimes. *Geophys. Res. Lett.*, **46**, 1014–1023.

Pfahl, S., and H. Wernli, 2012: Quantifying the relevance of cyclones for precipitation extremes. *J. Climate*, **25**, 6770–6780.

Sawada, M., and K. Ueno, 2021: Heavy winter precipitation events with extratropical cyclone diagnosed by gpm products and trajectory analysis. *J. Meteor. Soc. Japan*, **99**, 473–496.

So, K. W., C. Y. Tam, and N. C. Lau, 2022: Impacts of global warming on meiyu–baiu extreme rainfall and associated mid-latitude synoptic-scale systems as inferred from 20km agcm simulations. *Climate Dyn.*, **59**, 1849–1861.

Sodemann, H., C. Schwierz, and H. Wernli, 2008: Interannual variability of Greenland winter precipitation sources: Lagrangian moisture diagnostic and north atlantic oscillation influence. *J. Geophys. Res. Atmos.*, **113**, doi: 10.1029/2007JD008503.

Sprenger, M., and H. Wernli, 2015: The lagranto lagrangian analysis tool – version 2.0. *Geosci. Model Dev.*, **8**, 2569–2586.

de Vries, A. J., 2021: A global climatological perspective on the importance of rossby wave breaking and intense moisture transport for extreme precipitation events. *Wea. Climate Dyn.*, **2**, 129–161.

White, C. J., D. I. Domeisen, N. Acharya, E. A. Adefisan, M. L. Anderson, S. Aura, A. A. Balogun, D. Bertram, S. Bluhm, D. J. Brayshaw, J. Browell, D. Büeler, A. Charlton-Perez, X. Chourio, I. Christel, C. A. Coelho, M. J. DeFlorio, L. D. Monache, F. D. Giuseppe, A. M. García-Solórzano, P. B. Gibson, L. Goddard, C. G. Romero, R. J. Graham, R. M. Graham, C. M. Grams, A. Halford, W. T. Huang, K. Jensen, M. Kilavi, K. A. Lawal, R. W. Lee, D. MacLeod, A. Manrique-Suñén, E. S. Martins, C. J. Maxwell, W. J. Merryfield, Ángel G. Muñoz, E. Olaniyan, G. Otieno, J. A. Oyedepo, L. Palma, I. G. Pechlivanidis, D. Pons, F. M. Ralph, D. S. Reis, T. A. Remenyi, J. S. Risbey, D. J. Robertson, A. W. Robertson, S. Smith, A. Soret, T. Sun, M. C. Todd, C. R. Tozer, F. C. Vasconcelos, I. Vigo, D. E. Waliser, F. Wetterhall, and R. G. Wilson, 2022: Advances in the application and utility of subseasonal-to-seasonal predictions. *Bull. Amer. Meteor. Soc.*, **103**, E1448–E1472.

Yamashita, Y., R. Kawamura, S. Iizuka, and H. Hatsushika, 2012: Explosively developing cyclone activity in relation to heavy snowfall on the Japan sea side of central Japan. *J. Meteor. Soc. Japan*, **90**, 275–295.

Yamazaki, A., M. Honda, and H. Kawase, 2019: Regional snowfall distributions in a Japan-sea side area of Japan associated with jet variability and blocking. *J. Meteor. Soc. Japan. Ser. II*, **97**, 205–226.

Yiou, P., and M. Nogaj, 2004: Extreme climatic events and weather regimes over the north atlantic: When and where? *Geophys. Res. Lett.*, **31**, doi:10.1029/2003GL019119.